

**Nondestructive Spent Fuel Characterization with  
Semiconducting Gallium Arsenide Neutron Imaging Arrays  
Agreement Number DE-F07-98ID13633**

**John T. Lindsay, Douglas S. McGregor, and John C. Lee  
University of Michigan**

**Progress Report for Phase 2  
July 1, 1999 – June 30, 2000**

**Task 1. Fabricate an optimized GaAs(<sup>10</sup>B) detector**

Single element <sup>10</sup>B-coated bulk GaAs detectors have been fabricated and tested for efficiency. The single element devices have been fabricated from commercially available bulk GaAs wafers that have been thinned to only 200  $\mu\text{m}$ . The thin cross section reduces background gamma ray interaction interference. The devices have been fabricated such that they operate at low voltages, usually between 50-100 V. A method to apply thick films (up to 2  $\mu\text{m}$ ) of <sup>10</sup>B has been developed. Various <sup>10</sup>B-film thicknesses, ranging 0.1-1.84  $\mu\text{m}$ , have been deposited. Measured efficiencies follow theoretical calculations well,<sup>1</sup> and thermal neutron efficiencies approaching 4% have been measured.<sup>2</sup>

The <sup>10</sup>B-coated bulk GaAs devices thus far have withstood neutron fluences above  $10^{14}$  n/cm<sup>2</sup> without any noticeable degradation. Radiation resistance tests are presently ongoing, with devices being irradiated up to a total neutron fluence of  $10^{17}$  n/cm<sup>2</sup>. Epitaxial-based GaAs detectors show very strong signals under a zero bias condition<sup>3</sup> and offer a low power alternative to bulk GaAs devices. Yet, comparisons to high purity GaAs-based neutron detectors clearly indicate that semi-insulating (SI) bulk GaAs devices are far more radiation hard than epitaxial GaAs detectors.<sup>4</sup> As a result, SI bulk GaAs devices are being used for the final design.

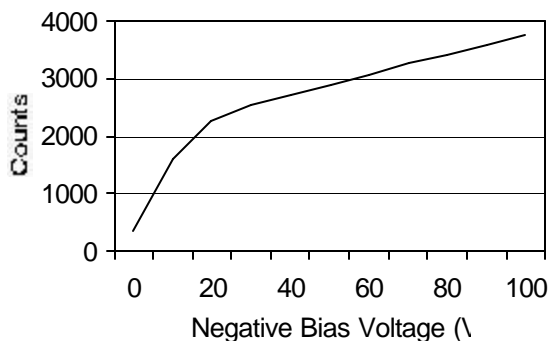


Figure 1. Neutron induced count rate as a function of bias voltage for the <sup>10</sup>B-coated GaAs detector under test

Detectors tested in a double diffracted thermal neutron beam yielded information as to the neutron detection count rate and detection efficiency. Figure 1 shows the count rate from a bulk GaAs device coated with 0.5  $\mu\text{m}$  of enriched <sup>10</sup>B irradiated in the Ford Nuclear Reactor (FNR) E-port. As can be seen, the count rate increases rapidly up to approximately 50 V of negative bias. Beyond 50 V, the counting efficiency increases only slightly. Higher bias voltages actually introduce more

electronic noise, hence the devices were generally operated between 50 and 130 V.

Several measurements were performed with the detector in a neutron beam from E-port. E-port is aligned directly with the corner of the FNR D<sub>2</sub>O moderator tank, hence the neutron flux and gamma-ray components are much higher than observed with the double diffracted beam at A-port. The measured neutron flux is approximately  $1.7 \times 10^6$  n/cm<sup>2</sup>-s and the gamma-ray exposure rate at E-port is 1.1 R/hr. Studies were performed with the devices shielded with various absorbers for neutrons and gamma-rays, including cadmium, borated high-density polyethylene (BHDP), and lead sheets. Shown in Figure 2 are the results of the single element device operated at a reverse bias of 80 V with no shielding (series 1), 2 inches lead (series 2), 2 inches of BHDP shielding (series 4), and 2mm cadmium/2 inches lead/2 inches BHDP (series 6). These measurements were performed to verify the detector was responding to the appropriate radiation type and expectations and to develop strategies for shielding the device for the spent fuel measurements.

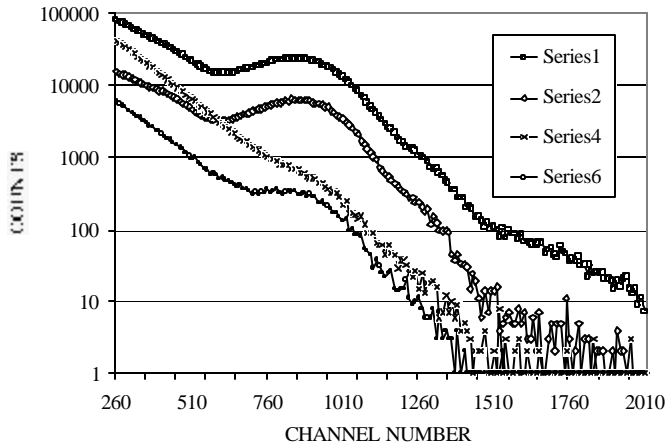


Figure 2. Comparison of spectra with a <sup>10</sup>B coated GaAs detector. Reverse bias = 80 V

gamma-ray (1.1 R/hr) and neutron field ( $10^6$  n/cm<sup>2</sup>-s) indicate that a very high neutron/gamma-ray discrimination ratio can be achieved. Measurements thus far show the n/g count rate ratio reaching 90 if the *LLD* is set high enough.<sup>2</sup> Lead shielding lowers the gamma-ray interactions significantly. The primary reason for the difference can be seen in Figure 2, in which the gamma-ray energy (channel number) demonstrates a near exponential decrease in count rate with increasing energy, an expected result for gamma-ray absorption in a material. However, the observed energy distribution of the charged-particle reaction products from <sup>10</sup>B(n,*a*)<sup>7</sup>Li reactions does not exponentially decrease with energy, primarily because the neutron interactions take place only at the detector surface and the observed energies are from absorption of the energetic charged-particle reaction products. In some cases, nearly all of the

The higher gamma ray environment of the E-port beam increases the interaction rate in the GaAs device, which is evident from the cadmium and BHDP filtered spectra. Yet, the gamma-ray discrimination ratio, with the lower level discriminator (*LLD*) set at 700 keV, is still very high, showing that the device serves as a self-discriminating neutron detector.

Discrimination tests in the mixed

charged-particle full energy is absorbed in the GaAs detector, thereby causing the appearance of a peak in the spectrum. Hence, a large separation in the energy spectrum between the gamma-ray events and the neutron-induced events becomes apparent near channel 660, and continues to separate further with higher energies. Channel 660 corresponds to approximately 725 keV. Shielding the detector with lead further enhances the  $n/g$  count ratio, in which the gamma ray component is reduced by a factor of approximately 2.5 over the neutron component for every two inches of lead. Hence, a two-inch lead shield increases the  $n/g$  discrimination ratio considerably.

Pixellated devices have also been fabricated. The pixels are 0.5 mm x 1 mm in size, and are arranged in a dual in-line design. Each line has 16 or 32 pixels, constituting a total of 32 or 64 pixels per device. The devices have been designed and cut such that they can be fit end to end without “dead” space. As a result, a very long array can be constructed with several devices laid lengthwise.

The new 32-element pixellated devices have been used in E-port and show an improved  $n/\gamma$  count ratio due primarily to their thinner design and a lower operating voltage (40 V). The pixellated detector has been used to image a variable thickness (1.0, 3.0, 4.5, 6.0, 7.3, 8.8, 10.0, 11.5, 12.5, and 13.5 mm) high density polyethylene (HDP) step wedge by scanning the detector across the step wedge. Figure 3 shows the detector response as a function of position across the step wedge for the first five wedge thicknesses using three minute counts. Figure 4 shows the spectra from the pixellated detector operated at 40V in E-Port. Shown are the raw

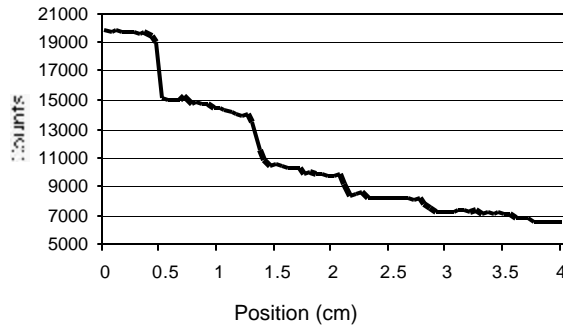


Figure 3. Three minute counts for a pixellated detector as a function of position across HDP step wedge with thicknesses of 1.0, 3.0, 4.5, 6.0, and 7.3

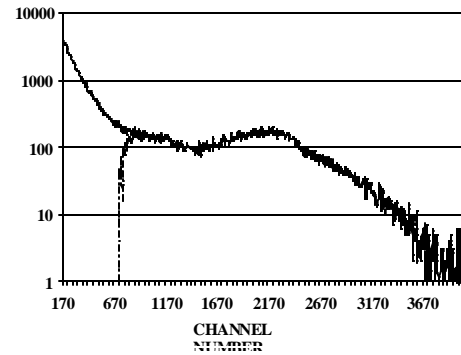


Figure 4. Total and gamma-ray subtracted spectra from a pixellated detector. Neutron-to-gamma-ray count ratio = 24.

spectrum (top) and the gamma-

ray corrected spectrum (bottom). For these measurements the  $n/\gamma$  count ratio was 24. This further demonstrates the detector's sensitivity to small changes in material thickness but also points out the need for long counts to develop good statistics. The neutron flux from the Sb/Be source is expected to be much lower than that available at E-port.

## Task 2. Build a 24-keV neutron collimator and Sb/Be source

A well shielded detector holding device and Sb/Be source have been designed from measurements made over the past year and are currently being constructed. An existing Sb/Be source is being used to determine the final source design geometry to maximize its use and minimize the noise signal from scattered neutrons and gamma-rays. A rotating/translation table has been designed to hold the spent fuel bundle and manipulate it in the beam. Half of the table was purchased during Phase 2 and the remainder will be purchased and assembled during Phase 3. Figure 5 illustrates the physical setup for the measurements for Phase 3, which will be performed in a hot cell with an irradiated control fuel bundle from the FNR.

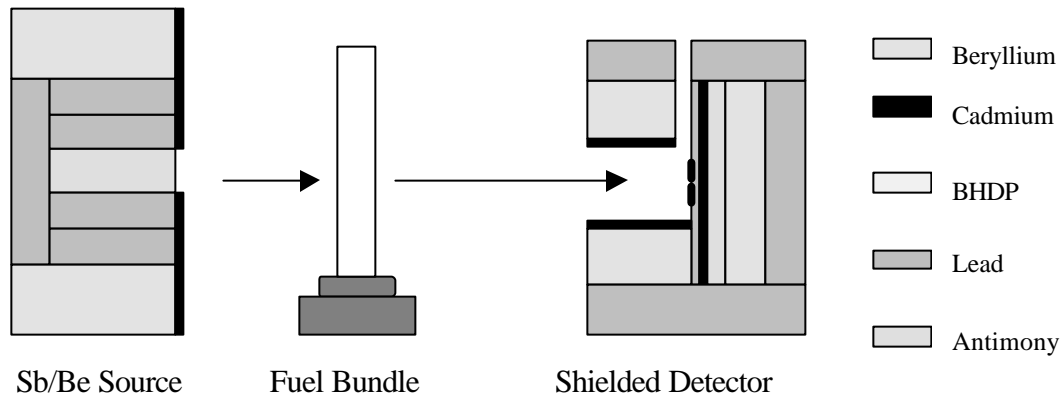


Figure 5. Physical setup for hot cell fuel bundle measurements.

## Task 3. Develop detector response algorithm and obtain spent fuel characteristics

This task involves the determination of fuel characteristics, including fuel burnup and fissile contents, in an irradiated fuel element from neutron reaction rates measured with  $\text{GaAs}(^{10}\text{B})$  detectors. For this purpose, we would like to determine the intensity and spectrum of the neutron flux emerging from the fuel element with and without a neutron source, in our case, an Sb/Be source. In particular, we would like to separately obtain contributions to the detector count rates from the 24-keV Sb/Be source neutrons, induced fission reactions, and spontaneous fission processes. Although an iron filter tends to provide a narrow window of neutron passage

around 24 keV, it is by no means a delta-function filter and we need to determine the neutron spectrum around this source energy of the Sb/Be source. For this task as well as for determining the fission contributions, we have developed a spectral unfolding technique utilizing the detector count rates measured with various filters. In addition to iron filters, we consider moderator films or plates placed between the fuel element and the detectors.

To provide a general framework for the unfolding approach, we consider a detector located at radius  $r$  from the axis of a neutron beam described by flux  $f(E)$  emerging from a fuel element and incident on the filter. We begin with an expression for the detector reaction rate  $R_i(r)$ , for the  $i^{th}$  filter, registered on the  $^{10}\text{B}$  film of absorption cross section  $\Sigma(E)$ :

$$R_i(r) = \int_0^\infty dE' \int_0^\infty dE f(E') K_i(r, E' \rightarrow E) \Sigma(E), \quad (1)$$

where  $K_i(r, E' \rightarrow E)$  is a kernel representing the neutron flux of energy  $E$  emerging from the filter and arriving at the detector due to a unit flux of energy  $E'$  incident on the filter. For a collimated beam of neutrons, the kernel  $K_i(r, E' \rightarrow E)$  may be interpreted<sup>6</sup> as the point spread function (PSF), on the detector plane, with the assumption that the filter is an isotropically scattering medium. Equation (1) may be recast in a simpler, intuitive form:

$$R_i(r) = \int_0^\infty dE f_i^*(r, E) \Sigma(E), \quad (2)$$

where  $f_i^*(r, E)$  represents the actual flux of neutrons of energy  $E$  incident on the detector:

$$f_i^*(r, E) = \int_0^\infty dE' f(E') K_i(r, E' \rightarrow E). \quad (3)$$

To obtain the information we seek, i.e., the flux  $f(E)$  for neutrons emerging from the fuel element, we define

$$A_i(r, E') = \int_0^\infty dE K_i(r, E' \rightarrow E) \Sigma(E) \quad (4)$$

representing the detector reaction rate associated with a unit flux of energy of energy  $E'$  incident on the filter and rewrite Eq. (1):

$$R_i(r) = \int_0^\infty dE' f(E') A_i(r, E'). \quad (5)$$

In terms of Eqs. (4) and (5),  $A_i(r, E')$  may now be interpreted as the detector cross section modulated by the filter PSF. Using a multi-group structure,  $j = 1, 2, \dots, N$ , Eq. (5) may be discretized:

$$R_i(r) = \sum_{j=1}^N A_{ij}(r) f_j, \text{ for the } i^{th} \text{ filter.} \quad (6)$$

For the solution to be feasible, the number  $N$  of the energy groups has to be constrained by the number of filters. Thus, for a relatively small number of filters, we need to consider a collection of detectors at different radial locations with respect to the incident collimated beam so that we may obtain sufficiently fine spectral information. Pixellated detectors may satisfy, in principle, this requirement in a natural way. In practice, however, it may be necessary to use a collection

of pixellated detectors, with different filter configurations, to create a modulated cross section matrix  $\mathbf{A}$  suitable for inversion. With each of these pixellated detectors providing a distinct reaction rate,  $R_i$ ,  $i = 1, 2, \dots, N$ , we obtain

$$R_i = \sum_{j=1}^N A_{ij} f_j, \quad i = 1, 2, \dots, N. \quad (7)$$

With the inversion of the modulated cross section matrix  $\mathbf{A}$ , we finally obtain the discrete flux spectrum:

$$\mathbf{f} = \mathbf{A}^{-1} \mathbf{R}. \quad (8)$$

During the reporting period, we have initiated measurements of the modulated cross section matrix  $\mathbf{A}$  under Task 2 and performed Monte Carlo calculations supporting the measurements. The measurements were made with several different filter arrangements at E-port of the FNR, where the average energy is 18 meV. We have used a different combinations of iron, cadmium, and polyethylene filters, with a single-element GaAs detector, concentrating on simple penetration measurements, which corresponds to  $A_i(r, E')$  for  $r = 0$  in Eq. (4). The Monte Carlo calculations for  $A_i(r, E')$  have been performed with the MCNP code<sup>7</sup> in a cylindrical geometry with a pencil beam of neutrons of different energies. The MCNP calculations indicate general agreement with the experimental data and the feasibility for the spectral unfolding approach outlined here. We note that the primary effect of a polyethylene filter is to slow down neutrons, for  $E > 1.0$  eV, thereby increasing the detector reaction rate. In contrast, the filter tends to act primarily as an absorber and attenuate the beam for neutrons with  $E < 1.0$  eV.

### Proposed Work for Phase 3

#### Task 1. Measure spent fuel characteristics of an irradiated FNR fuel element

##### 1. Optimized detector development

New GaAs detector designs are now underway and will be implemented. Theoretical models indicate that the new neutron detector designs can increase the maximum efficiency up above 12%, an increase of 3 times greater than the present design. The detectors are also being irradiated under various conditions to determine radiation hardness to gamma rays, neutrons and charged particles. The radiation hardness results will be compared with results for similar devices fabricated from Si. The pixellated devices will be connected to miniaturized readout electronics and driven as stand-alone plug-in chips.

##### 2. Three-dimensional fuel bundle measurements

The rotate/translate table will be used to move the fuel bundle through the Sb/Be neutron beam while data are taken from the 64 (minimum) pixel arrays and placed in a computer buffer. After traversing the full width of the fuel bundle, the fuel bundle will be rotated three degrees and another profile taken. The 120 profiles will be used to develop a 3-D

computerized reconstruction of the localized fuel characteristics of the bundle. These images will be developed with and without the neutron beam and with a series of filters to assist in the assay of the fissile contents. The fissile contents will be determined through the spectral unfolding formulation developed in Phase 2. These detailed profiles will be taken at several longitudinal locations along the fuel bundle to look for expected variations. In addition longitudinal measurements will be used with a fixed source and fuel bundle orientation and movement of the detector array to gather off-axis scatter information for use in the modeling discussed under Task 2.

## **Task 2. Optimize the computational scheme to determine spent fuel characteristics**

### **1. Experimental determination of the modulated cross section matrix $\mathbf{A}$**

Once an Sb/Be source is fabricated to provide 24-keV neutrons, we will concentrate on using the source with a suitable iron filter to obtain the intensity and spectral information associated with the source neutrons. We will also determine the neutron flux emerging from a mockup of FNR fuel elements using varying combinations of filters. We will make full use of pixellated GaAs detectors during the coming year.

### **2. Simulation of spent fuel measurements**

MCNP calculations, combined with the WIMS lattice physics code,<sup>8</sup> will be used to simulate the isotopic distribution in the fuel assembly and the detector geometry. The calculated matrix  $\mathbf{A}$  will be benchmarked to actual measurements. We will use the spectral unfolding methodology developed in Phase 2 to obtain discrete spectral data and obtain contributions from spontaneous and induced fission processes. The overall spectral unfolding methodology and spent fuel assay techniques will be verified through MCNP calculations.

## References

1. D. S. McGregor, J. T. Lindsay, C. C. Brannon, and R. W. Olsen, "Semi-Insulating Bulk GaAs Thermal Neutron Imaging Arrays," *IEEE Trans. Nucl. Sci.*, **43**, 1358-1364 (1996).
2. D. S. McGregor, R. T. Klann, H. K. Gersch, and Y-H. Yang, "Thin-Film-Coated Bulk GaAs Detectors for Thermal and Fast Neutron Measurements," *2nd International Workshop on Radiation Imaging Detectors*, Freiburg, Germany, July 2-6, 2000; to appear in *Nucl. Instrum. Method* (2000).
3. D. S. McGregor, S. M. Vernon, H. K. Gersch, S. M. Markham, S. J. Wojtczuk and D. K. Wehe, "Self-Biased Boron-10 Coated High Purity Epitaxial GaAs Thermal Neutron Detectors," submitted to *IEEE Trans. Nucl. Sci.*, November, 1999.
4. H. K. Gersch, D. S. McGregor, and D. K. Wehe, "A Study of the Effect of Incremental Neutron Fluences Upon the Performance of Self-Biased  $^{10}\text{B}$ -Coated High-Purity Epitaxial GaAs Neutron Detectors," to be presented at the *2000 IEEE Nucl. Science. Symp.*, to be held in Lyon, France, Oct. 15-20, 2000.
5. D. S. McGregor, J. T. Lindsay, Y-H. Yang, and J. C. Lee, "Bulk GaAs Based Neutron Detectors for Spent Fuel Analysis," No. 8827, *8th International Conference on Nuclear Engineering*, Baltimore, MD, April 2-6, 2000.
6. J. Park, J. T. Lindsay, and J. C. Lee, "Transport Calculation of Scattering Line Spread Function for Neutron Radiography," *Trans. Am. Nucl. Soc.*, **80**, 83 (1999).
7. J. F. Briesmeister, Ed., "MCNP – A General Monte Carlo N-Particle Transport Code, Version 4A," LA-12625, Los Alamos National Laboratory (1993).
8. J. R. Deen, W. L. Woodruff, and C. I. Costescu, "WIMS-D4M User Manual, Rev. 1," ANL/RERTR/TM-23, Argonne National Laboratory (1997).